MATERIALS SCIENCE

A readily programmable, fully reversible shape-switching material

Matthew K. McBride[1], Alina M. Martinez[2], Lewis Cox[3], Marvin Alim[2], Kimberly Childress[1], Michael Beiswinger[1], Maciej Podgorski[1,4], Brady T. Worrell[1], Jason Killgore[3], Christopher N. Bowman[1,2]*

Liquid crystalline (LC) elastomers (LCEs) enable large-scale reversible shape changes in polymeric materials; however, they require intensive, irreversible programming approaches in order to facilitate controllable actuation. We have implemented photoinduced dynamic covalent chemistry (DCC) that chemically anneals the LCE toward an applied equilibrium only when and where the light-activated DCC is on. By using light as the stimulus that enables programming, the dynamic bond exchange is orthogonal to LC phase behavior, enabling the LCE to be annealed in any LC phase or in the isotropic phase with various manifestations of this capability explored here. In a photopolymerizable LCE network, we report the synthesis, characterization, and exploitation of readily shape-programmable DCC-functional LCEs to create predictable, complex, and fully reversible shape changes, thus enabling the literal square peg to fit into a round hole.

INTRODUCTION

Shape-changing polymeric materials convert stimuli-responsive changes in the polymer structure to alterations in bulk, micro, and nanoscale shapes dynamically. Leveraging these shape changes offers control over optical (*1*–*3*), mechanical (*4*), frictional (*5*), and structural (*6*) properties in response to a variety of external stimuli including heat (*1*, *7*, *8*), light (*9*–*13*), pH, and chemical activation (*14*, *15*). With this diversity, proposed applications include numerous biomedical applications (*16*), four-dimensional printing (*17*, *18*), autonomous folding (*19*), robotics (*5*), optical elements (*20*), artificial muscles (*21*), and a myriad of other emerging applications. Converting an applied stimulus into a desired shape change has been achieved through a variety of mechanisms including glass transition temperatures, phase transitions, liquid crystalline (LC) transitions, dynamic covalent chemistry (DCC), and noncovalent intermolecular interactions. All of these physical phenomena, incorporated into an appropriate polymeric system, enable varying degrees of stimuli-responsive control over the shape including one-way, two-way, multishape, or permanent shape change. Despite this plethora of work, problems continue to persist in programmability and time scale of shape change (*22*, *23*).

Although their longer characteristic response times make them inappropriate for many applications, of these approaches, LC networks and LC elastomers (LCNs and LCEs, respectively) constitute two of the most promising classes of materials currently used as fully reversible shape-changing materials because their molecular order is directly translated into macroscopic shape. The underlying molecular order in LCNs, programmed through a variety of techniques (*7*, *24*–*26*), leads to phase- and temperature-dependent anisotropic shape changes when exposed to an order-disrupting stimulus such as heat, solvent, or light. The mechanical properties dictate the extent of shape change achieved with lower cross-linked materials (LCEs) having larger amplitudes and stiffer materials (LCNs) having faster response times and larger stroke (*27*). Covalent adaptable networks, or networks that alter their covalent connectivity in response to an applied stimulus (*28*), are a viable means to create readily reprogrammable LCEs, as shown by the pioneering works of Pei and coworkers (*29*–*31*) with additional work from other groups (*32*, *33*) that implement thermally triggered DCC in LCEs. Although implemented successfully, thermally induced bond exchange is intrinsically linked to the thermotropic LC behavior, thereby severely limiting the ability to chemically anneal and shape program in each phase. The first demonstration of using light-facilitated bond exchange to decouple the thermotropic behavior of LCNs used heat to decrease the birefringence and to generate surface features through bond-stabilized disruption of LC order; however, bond exchange–stabilized alignment was not demonstrated as the overall LCN alignment was programmed before polymerization (*34*). In the pursuit of more complex and controllable shape changes in LCEs, we have developed a photopolymerizable LCE that uses light-triggered DCC to dynamically stabilize the alignment. Light initiation decoupled the LC behavior and alignment from the dynamic bond exchange process while simultaneously enabling spatial patterning of that decoupled process and the associated LC alignment.

RESULTS

Light-facilitated bond exchange is achieved here by incorporating radical-mediated addition-fragmentation chain transfer (AFT) functionalities into the backbone of acrylate-terminated LC oligomers (Fig. 1A), bond exchange mechanism shown in fig. S1. A thiol-Michael addition reaction enabled the facile installation of the desired functionality by the addition of allyl dithiol into the oligomerization. In contrast to other work, the thiol-Michael addition provided an easily accessible route to forming processable acrylate-capped oligomers as opposed to forming the network directly with this reaction, as done previously (*7*, *35*). Allyl dithiol, as the thiol monomer, reacted with a slight stoichiometric excess of mesogenic diacrylate (RM82) and neopentyl glycol diacrylate (NPGDA), resulting in acrylate end-capped oligomers containing an AFT-capable allyl sulfide, which were then photopolymerized into a cross-linked network. Radicals generated from photoinitiators during light exposure catalyzed the polymerization of

[1]Department of Chemical and Biological Engineering, University of Colorado Boulder, 596 UCB, Boulder, CO 80309, USA. [2]Materials Science and Engineering, University of Colorado Boulder, 596 UCB, Boulder, CO 80309, USA. [3]Applied Chemicals and Materials Division, Material Measurement Laboratory, National Institute of Standards and Technology, Boulder, CO 80305, USA. [4]Faculty of Chemistry, Department of Polymer Chemistry, Maria Curie-Sklodowska University, Gliniana Street 33, 20-614 Lublin, Poland.
*Corresponding author. Email: christopher.bowman@colorado.edu

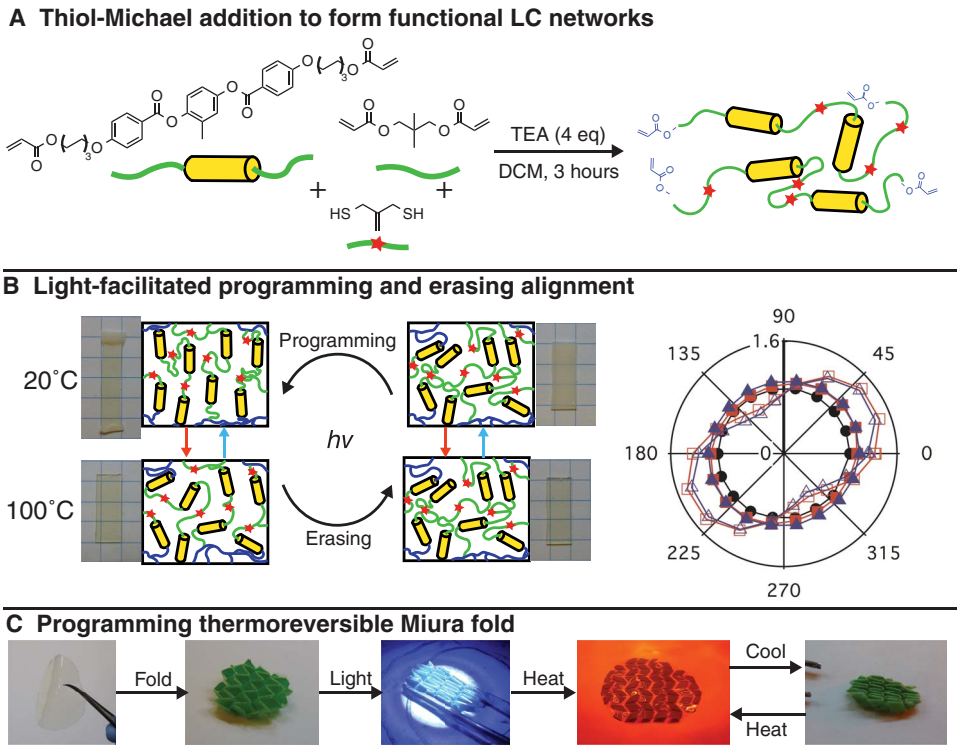

Fig. 1. Photopolymerizable AFT-LCEs were programmable and erasable. (**A**) Thiol-Michael addition reaction scheme to install RAFT functional groups into photopolymerizable acrylic oligomers. (**B**) LCEs were aligned and subsequently erased by applying a mechanical bias (programming) or a thermal disruption (erasing) coupled with light (*hv*, 30 mW/cm^2, 320 to 500 nm). The polar graph presents the polarized Fourier transform infrared spectroscopy (FTIR) peak area corresponding to C–H on the aromatic core (3350 to 3300 cm^{-1}) at various light polarization angles. Each line represents the following: as-polymerized polydomain (●), programmed (30-s *hv*, 100% strain, cycle 1, □), erased cycle 1 (30-s *hv*, 120°C, cycle 1, ■), programmed (30-s *hv*, 100% strain, cycle 2, △), and erased (60-s *hv*, 120°C, cycle 2, ▲). Programming was done parallel to 90°. (**C**) Example of programming process starting from a polydomain 250-μm-thick polymer. The polymer was folded by hand and programmed with 320 to 500 nm (100 mW/cm^2) coupled with gentle heating (30° to 40°C). Subsequent thermal cycling resulted in the network unfolding at high temperatures and folding during cooling (movie S1).

the acrylate end groups on the oligomers to form the polymer network on demand. The addition of NPGDA reduces the phase transition in a continuous manner as the amorphous content is increased, and the exemplary ratio of 1:0.5 RM82/NPGDA was chosen to yield a clearing temperature of 80°C, as determined by microscopy and mechanical characterization (fig. S2). AFT units, specifically allyl sulfides, participate in a radical-mediated bond exchange reaction that is initiated with latent, radical-generating photoinitiators that exist throughout the polymer network. The corresponding bond exchange process allows an otherwise elastic, cross-linked LCE to, in a transient and stimuli-responsive manner, behave as a viscoelastic liquid. Comparing it to traditional definitions of polymeric materials, AFT effectively bridges the gap between a thermoset and thermoplastic material, enabling us to separate the shape-changing behavior from the programming behavior through the application of light.

Unique to this work, the temporal control provided by light separated the AFT exchange from the thermotropic LC behavior. As a consequence, AFT exchange stabilized the LC alignment associated with the equilibrium state at the given temperature and mechanical strain. Applying this concept, the alignment was rewritten in Fig. 1B over multiple cycles and observed with polarized FTIR. A schematic and representative images of this process are provided in Fig. 1B. The equilibrium molecular alignment was observed by polarized FTIR over multiple programming and erasing cycles (Fig. 1B). Here, the C–H stretch of the aromatic core is aligned upon AFT-activating light exposure in the strained state as indicative of stabilization of the monodomain structure, while exposure and the associated AFT activation in an unstrained state at elevated temperature lead to the formation of a polydomain LCE structure in which the average bond orientation was again stochastically oriented. All polarized FTIR measurements were performed at ambient temperature under an unstrained condition, thereby representing the final state. Extending this concept beyond simple mechanical stretching, AFT exchange programmed more complex folded and bulk shapes. Complex folding shapes, such as the Miura fold pattern, were programmed, as shown in Fig. 1C, which was simply folded by hand and irradiated with 320 to 500 nm (100 mW/cm^2) or 5 min with occasional flipping to ensure uniform light exposure on each surface. Upon heating, the Miura fold would open into a flat sheet and return to the folded state after cooling back to room temperature, repeatedly taking on each of the shapes as dictated by the temperature (movie S1); however, without light exposure, the Miura fold returned to its flat shape and remained flat during cooling. Thus, light exposure and the corresponding AFT activation are essential to the process. AFT was also used to reprogram the LC phase shape in a manner analogous to Fig. 2B; however, more complex shapes were used instead of simple stretching (fig. S3). Light exposure programmed a twist from a flat shape that was subsequently erased and reprogrammed into a folded object, thereby demonstrating robust reconfiguring ability. In addition, the isotropic shape, that is, the shape that the object takes on at elevated temperature, was able to be set during the initial photopolymerization, while the LC shape, that is, the shape that the object takes on at ambient temperature in the nematic phase, is programmable by

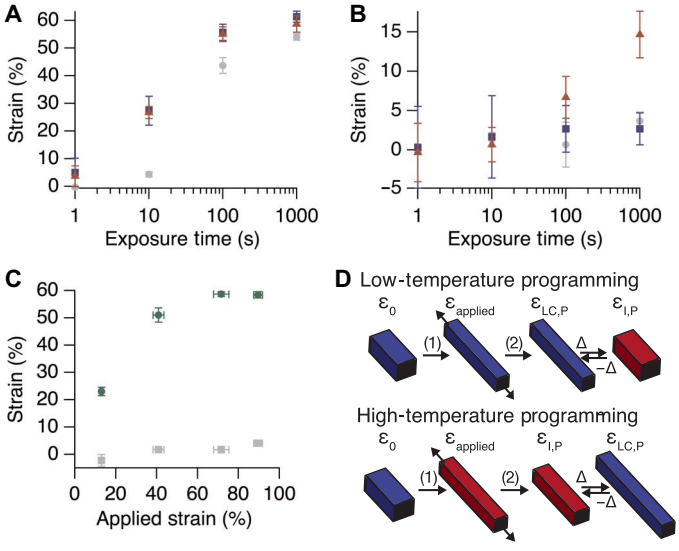

Fig. 2. Final LC and isotropic phase shape after programming under various conditions. (**A**) Strain relative to initial shape in the LC state after programming for various exposure times (320 to 500 nm, 30 mW/cm^2) at 25°C (●), 67°C (▲), and 120°C (■). Programming strain was set at 45 ± 10% except for 120°C samples, which were set at 15 ± 5%. (**B**) Strain in the isotropic state measured at 120°C after programming for various exposure times (320 to 500 nm, 30 mW/cm^2) at 25°C (●), 67°C (▲), and 120°C (■). (**C**) Strain in LC state (●) and isotropic state (■) after programming (320 to 500 nm, 30 mW/cm^2, 300 s) at room temperature at various exposure strains. (**D**) Schematic representation of the experiment. Beginning from ε_0, the sample is stretch (1) to the applied strain ($\varepsilon_{applied}$) and heated to the appropriate temperature (blue denotes 25°C and red denotes both 67° and 120°C). After light exposure and release of strain (2), the sample was thermally cycled to measure the programmed strain in the LC phase ($\varepsilon_{LC,P}$) and isotropic phase ($\varepsilon_{I,P}$).

AFT exchange. This approach was further used to program a square peg shape at room temperature from an LCE polymerized as a cylindrical peg to enable the proverbial "square peg" to fit into a "round hole" (movie S2 and fig. S4) in a completely reversible and repeatable manner when heated. Here, the LCE reversibly takes on a stable square peg shape under ambient conditions while morphing into a cylindrical peg at elevated temperatures that fits into the round hole. Notably, for all the examples studied here, the isotropic phase shape remains unaffected by programming of the aligned shape in the LC phase. As such, the AFT was easily used to program the LC phase shape without significantly changing the isotropic shape, indicating that the effects from the AFT process are only manifested in the LC phase if programming is done in that state.

To explore further how AFT affects the permanent LC and isotropic phase shapes, the tensile strain, $\varepsilon_{applied}$, and the temperature applied during programming were varied while measuring the resulting strains relative to the initial shape, ε_0, at both 100° and 25°C, $\varepsilon_{I,P}$ and $\varepsilon_{LC,P}$, respectively (Fig. 2, A and B). The $\varepsilon_{LC,P}$ reaches a maximum near 60% strain under all programming temperatures for this system, but we note that this formulation is not optimized, and the value is relatively low compared to other LCE formulations, which can reach well over 100% (*36*). To improve this, lowering the cross-linking density by increasing the oligomer length will subsequently increase the maximum $\varepsilon_{LC,P}$. The approach taken here of using AFT to enable reprogrammability with spatiotemporal control is one that is generalizable across the LCE and LCN parameter space. For any LC system into which an allyl sulfide could be incorporated, we would readily envision that the same benefits illustrated here would be available in those systems as well, whether they had fast response times, higher elongation to break, improved optical performance, or some other desired characteristics. The maximum $\varepsilon_{LC,P}$ appears to be independent of programming conditions and is limited by the base LC in the material within which the AFT moieties are incorporated. This limit also corresponds to the approximate end of soft elasticity in the stress-strain curve, leading us to conclude that the sample has reached the monodomain state (fig. S5). Polarized microscopy also confirmed the formation of a monodomain structure from a polydomain after programming (fig. S6). Work from Terentjev's group previously reported that the soft elasticity characteristic of LCEs during deformation is attributed to aligning the randomly oriented domains into a single monodomain with stress primarily concentrated in the domain boundaries to minimize the free energy of the system (*37*). This analysis led to the hypothesis that the AFT process proceeded in a manner that relaxed the concentrated stress at domain boundaries as the bond exchange process worked to minimize the overall free energy of the system. The noticeable lack of programmed strain in the isotropic phase, as mentioned above, also supported this hypothesis. Since the stress was concentrated in the domain walls, the AFT that caused measurable shape change in the isotropic phase occurred in a relatively small volume of the polymer, where the stress is concentrated in the LCE. This is further evidenced by how AFT programs the shapes when activated at various temperatures. Programming at 120°C leads to the polymer adopting a monodomain in the LC phase and conforming, almost completely, to the applied strain in the isotropic phase; however, samples programmed in the LC phase (25° and 67°C) showed little, if any, programmed strain in the isotropic phase. Once the programming temperature was increased above the phase transition (80°C), the LCE behaved as an amorphous network with the stress more uniformly distributed throughout the network, leading to equally uniform stress relaxation in the entire volume of the material.

The marked temperature effect on the mechanical properties is further observed by dynamic mechanical analysis (DMA) and stress relaxation behavior in these LCEs. DMA shows a distinct minimum in the rubbery modulus below the phase transition of the materials that has been attributed to the low rotation barrier of the LC domains above the glass transition (fig. S2) (*38*). With this behavior in mind, the stress relaxation was monitored with and without light exposure at 25°, 67°, and 120°C (fig. S7) to access different physical states (glassy and rubbery), as well as different LC phases. According to rubbery elasticity, the increased long–time scale relaxation modulus indicates that more chains are elastically active at higher temperatures, particularly above the phase transition. Bond exchange in samples with a higher concentration of elastically active chains resulted in larger changes in the isotropic shape, whereas samples stretched to within or just above the soft-elasticity plateau in the LC phase show little change in their isotropic shape. Programming near the storage modulus minimum (67°C) requires a significantly reduced exposure time and strain to reach a monodomain sample without significantly changing the isotropic shape. This behavior is attributed to increased mobility as the residual glass transition effects dissipate near and just below this temperature. Furthermore, stress relaxation in this manner is expected to occur if the stress and thereby measurable stress relaxation are localized in the domain walls in the LC phase, while the stress is more uniformly distributed in the isotropic phase.

Programming LC alignment in the isotropic state depended significantly on the external bias applied to the LCE. Most notably, the LCEs were readily aligned when the bond exchange was initiated under load, but the alignment was completely erased when the bond exchange was

initiated in the absence of any external load. AFT was used to program a monodomain in the isotropic phase (Fig. 2A) similar to the sample programmed in the LC phase at 67°C. According to our hypothesis, this similarity arose from both samples reaching a similar monodomain configuration; however, the mechanism for reaching that state is slightly different. The sample programmed in the LC phase resulted in stresses concentrated at the interface of the domains to be relaxed, leading to a monodomain structure and very little residual $\varepsilon_{I,P}$. In contrast, the samples programmed in the isotropic phase (100°C) distributed the stress more evenly throughout the network, causing significant $\varepsilon_{I,P}$ and a monodomain structure in the LC phase. The monodomain is the result of incomplete stress relaxation during AFT as it is limited by photoinitiator content (fig. S7 does not show 100% stress relaxation in the isotropic phase). Residual stress within the network directed the LC alignment upon cooling into the LC phase after AFT. A similar effect was reported in semicrystalline AFT networks where elongated polymer chains are not relaxed during AFT nucleated local crystallization (*39*). Without any externally applied stress, the internal stresses generated by the phase transition are erased during the stochastic bond exchange, ultimately leading to a polydomain structure when cooled (fig. S8).

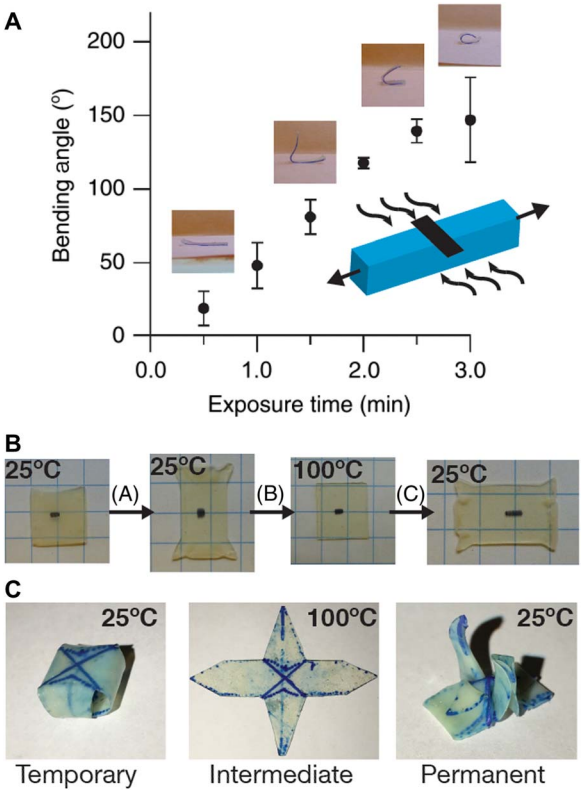

Fig. 3. Controllable shape changes in AFT-LCEs. (**A**) With inclusion of a photoabsorber, programming of optically thick samples results in thermoreversible bending. The graph depicts bending angle after various irradiation times at room temperature (365 nm, 50 mW/cm^2; 20% strain). (**B**) Starting from a thermally quenched, programmed LCE, the temporary shape was programmed by stretching perpendicular to the light programmed direction (A). The molded sample was then heated (B), revealing the intermediate square shape, and upon cooling, spontaneously returned to the light-programmed LC shape (programming, 365 nm, 30 mW/cm^2). (**C**) A box was programmed as the temporary shape and unfolded after heating. After cooling, the LCE autonomously folded into a swan, as previously programmed with light (365 nm, 50 mW/cm^2; 300 s).

With this analysis in mind, multistep programming procedures would enable the isotropic shape to be readily separated from the LC phase shape and initial, as-polymerized shape (fig. S9).

DISCUSSION

With a complete understanding of the stress relaxation process, the achievable shape change limits were exploited in these materials. Light offers a unique spatial and temporal control of this process that was used to develop bent and folded structures by simply patterning the alignment. Figure 3A depicts spatially disparate LC domain alignment on each face, resulting in bending with more complex structures developed in fig. S10 and surface patterns in fig. S11. In addition, the thermomechanical properties enable one-way shape memory where a third, temporary shape was readily programmed by quench cooling a programmed AFT-LCE below its glass transition, preventing the LC from self-organizing. After warming to room temperature, samples maintained a stable polydomain orientation that was further reshaped into a temporary shape, as demonstrated in Fig. 3 (B and C). Subsequent heating returned the temporary shape to the isotropic phase shape, and cooling returned it to the AFT programmed LC phase shape. This process works for more complicated structures as well. A box that unfolds after heating and refolds into an origami swan after cooling back into the LC phase was formed (Fig. 3). Thus, this approach enables three distinct shapes to be programmed independently with the thermally quenched, temporary shape, LC phase shape, and isotropic phase shape.

Beyond programming of macroscopic topologies, shape-switching behavior at smaller, submicrometer length scales offers unique opportunities

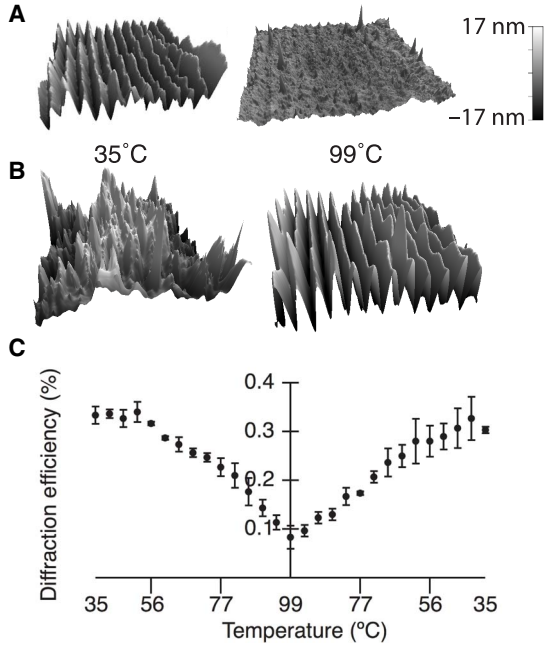

Fig. 4. Thermoreversible shape change programmed by nanoimprinting. (**A**) Atomic force microscopy (AFM) images taken at 35° and 99°C for a diffraction grating programmed at 55°C with 3 MPa and 300- to 400-nm (20 mW/cm^2) light for 1 min. The images are 10 μm × 10 μm with the *z* axis color scale shown at the right (17 to −17 nm). (**B**) AFM images taken at 35° and 99°C of a diffraction grating programmed at 99°C, followed by a second, flat programming step at 55°C with same irradiation conditions as in (A). (**C**) Diffraction efficiency as a function of temperature for grating programmed at 55°C. This sample corresponds to the AFM images shown in (A).

to equip smart surface technologies with switchable wetting, optical and adhesive properties, among others. To investigate the potential of LCEs to switch between programmed submicrometer surface topographies, we used a nanoimprint lithography (NIL) system to imprint grating patterns, with a periodicity comparable to the wavelength of visible light, onto LCE surfaces. The bond exchange resulted in thermoreversible diffraction gratings, as shown in Fig. 4, where the programming temperature determined the thermoreversibility of the grating. For the diffraction gratings programmed in the LC phase, the repeating structures and the corresponding diffraction pattern are markedly diminished when heated to the isotropic state, only to reappear when cooled, with the ability to cycle repeatedly between these optically active and optically passive states. Surface features were mapped at various temperatures and coupled with temperature-dependent measurements of the diffracted light. Although the diffracted spot does not completely disappear, the programming conditions could be optimized (pressure, temperature, exposure, etc.) to minimize the surface feature. Conversely, the diffraction grating was also imprinted in the isotropic state, generating a larger pattern height, the periodicity of which is disrupted when cooled into the LC phase. To remove these surface features at ambient temperature, a second programming step was done in the LC phase using a flat silicon wafer to compress the diffraction grating flat. Using this programming routine, AFM (Cypher S, Asylum Research) images show that the repeating pattern was replaced with a randomly rough surface; however, this roughness coupled with a slight opacity from the polydomain structures prevented accurate measure of the diffraction efficiency due to light scattering. Despite scattering at low temperatures, a clear diffraction spot was observed at high temperatures. In either case, the LCEs demonstrated an impressive ability to generate thermoreversible, optically active, nanoscale surface features that could be used to control the surface properties of the material.

In summary, we have developed a photopolymerizable, thermoreversible shape-changing material that was repeatedly programmable with mechanical force or heat coupled with light. This repeated and facile programming is ultimately enabled because the DCC was initiated independent from the thermotropic LC behavior. Decoupling the DCC and the LC behavior allowed various shapes to be programmed in the LC phase and isotropic phase nearly independently. Because the DCC chemically anneals the polymer network toward an equilibrium state, the order was readily and repeatedly programmed (at low temperatures) or erased (above the phase transition), thus enabling a broad array of programming conditions and steps to give complex thermoreversible shape changes.

MATERIALS AND METHODS

Materials

1,1′-(2-Methyl-1,4-phenylene) ester 4-[[6-[(1-oxo-2-propen-1-yl) oxy]hexyl]oxy]-benzoic acid (RM82) was obtained from Wilshire Technologies. 3-Chloro-2-(chloromethyl)-1-propene, potassium ethyl xanthogenate, NPGDA, dichloromethane (DCM), and triethylamine (TEA) were purchased from Sigma-Aldrich. Ethylenediamine was obtained from TCI America. All chemicals were used as received unless otherwise noted.

Synthesis of allyl dithiol

2-Methylene-1,3-propanedithiol (allyl dithiol) was synthesized according to previously reported procedure (*34*). In a 1000-ml round-bottom flask with a stir bar, potassium ethyl xanthogenate (56.4 g, 352 mmol) was dissolved into ethanol (500 ml). 3-Chloro-2-(chloromethyl)-1-propene (18.5 ml, 160 mmol) was added dropwise, and the reaction was left overnight. The solids were then removed with filtration, and ethanol was removed using a rotary evaporator. Diethyl ether (200 ml) and water (100 ml) were added to the yellow residue, and the organic phase was removed and washed with water (2×, 100 ml), washed with brine (1×, 100 ml), and dried over sodium sulfate. The ether was removed under a vacuum, resulting in the protected allyl dithiol as a yellow low-viscosity liquid used without further purification in the next step. In a flame-dried, 50-ml round-bottom flask with an addition funnel under argon, the protected allyl dithiol (10 g, 33.8 mmol) was added over 30 min to anhydrous ethylenediamine (16 ml) held at 20°C. After 3 hours, the reaction mixture was slowly added to 200 g of ice and 32 ml of sulfuric acid (concentrated). The milky white solution was extracted with diethyl ether (2×, 200 ml). The organic phases were combined and extracted with 2 M sulfuric acid (2×, 100 ml) and brine (1×, 100 ml). The organic phase was then dried over sodium sulfate, filtered, and concentrated in vacuo, resulting in a slightly yellow low-viscosity liquid with an extremely foul odor. The allyl dithiol was distilled immediately before use (60°C, 0.1 mmHg, 2.6 g, 60% yield). Impurities were observed if allowed to sit overnight after purification. ^{1}H nuclear magnetic resonance (NMR) (400 MHz, $CDCl_3$, 25°C): 4.99 (broad singlet, 2H), 3.37 to 3.34 (multiplet, 4H), 1.48 (triplet, J = 8.15 Hz, 2H).

Purification of NPGDA

NPGDA was purified via flash chromatography. Column conditions were 10% ethyl acetate in hexanes using a Biotage Isolera One. Inhibitor, 4-methoxyphenol (MEHQ), was added in a 100–parts per million (ppm) concentration.

Synthesis of diacrylate oligomers

Diacrylate oligomers were synthesized via a base-catalyzed thiol-Michael addition in a manner similar to those previously reported (*34*). In an open 100-ml round bottom flask with a mechanical stir bar, butylated hydroxytoluene (9 mg, 1000 ppm), RM82 (6625 mg, 9.858 mmol), and NPGDA (1046 mg, 4.929 mmol) were dissolved into DCM (30 ml, 0.5 M), followed by the addition of allyl dithiol (1600 mg, 13.308 mmol). TEA (8.24 ml, 59.14 mmol) was added, and the reaction mixture was allowed to stir for 16 hours, followed by the removal of DCM and TEA in vacuo. The resulting viscous liquid was dissolved in DCM (200 ml) and washed with 1 M HCl (2×, 100 ml) and brine (1×, 100 ml), followed by drying with sodium sulfate and removal of DCM in vacuo, which produced a white semisolid resin. NMR was used to confirme the consumption of thiols and determine the average number of repeat units through end group analysis of acrylic protons compared to allylic allyl sulfide protons. A molar ratio of 1:0.5:1.35 (RM82/NPGDA/allyl dithiol) was used for all results shown unless explicitly stated.

Photopolymerization of polydomain films

Oligomers (400 mg) were dissolved in 4 ml of DCM. Photoinitiators (Irgacure 819, Irgacure 651, and Irgacure 2959) were dissolved in DCM (10 mg/ml) and added to the dissolved oligomers in the appropriate proportions. Irgacure 819 and Irgacure 651 were added at 1.5 weight % (wt %) (6 mg, 600 μl) and 1 wt % (4 mg, 400 μl). Irgacure 2959 was added for multiple exposure experiments at 1 wt % (4 mg, 400 μl). The dissolved resin was then deposited onto a Rain-X–coated glass at 160°C on a hotplate and allowed the DCM to evaporate open to air (30 min) with occasional stirring. The resin was then pressed between two Rain-X–coated glass plates with 500-, 250-, or 140-μm plastic spacers

and heated to 160°C on a hotplate for 5 min to erase residual stress. Photopolymerization was then performed at 110°C on a hotplate (±10°C measured with a thermocouple) with 400- to 500-nm (50 mW/cm^2) light (Exfo Acticure Hg Bulb) for 3 min. The resulting slightly yellow polymer network had a slight haze, confirming a polydomain structure. Thermal cycling led to a minimal shape change.

Programming of complex shape changes

Programming of folded and twisted shapes was done by mechanically molding a polydomain film, by hand, into the desired shape and irradiating it with 320- to 500-nm (50 to 100 mW/cm^2) light from a mercury bulb light source. For the Miura fold demonstration, pieces of label tape were added to aid in folding and visualization of the object and thus were not permanently attached to the film. For the square peg demonstration, a polydomain LCE was photopolymerized in a cylindrical glass vial and removed after curing under conditions similar to those described above. The cylinder was molded by hand into a rectangle (square peg) before light irradiation that programmed the rectangular shape in the LC phase while maintaining the cylindrical shape in the isotropic phase.

Measurement of strain after programming

LC and isotropic shape measurements were obtained by image analysis [ImageJ, National Institutes of Health (NIH)]. Two circular dots were marked on polydomain films (250-μm thickness, 3.15 × 10 mm) approximately 2 mm apart. Images were taken using a Panasonic Lumix camera at room temperature (20°C, approximately room temperature) for LC strain (ε_0) and 120°C (±10°C measured with a thermocouple) hotplate for isotropic strain (ε_0; isotropic and LC were approximately equal in all cases). The films were then placed in a stretching device and stretched to a predetermined length and irradiated with 320 to 500 nm (50 mW/cm^2) for the prescribed amount of time. For samples irradiated at 67° and 120°C, an oven with a window was used to control the temperature. The temperature was measured with a thermocouple placed next to the sample, and the temperature was allowed to equilibrate for 30 min before exposure. The accuracy of the programming temperature measurement was estimated as ±1°C. The samples were removed from the stretching device, heated to 120°C on a hotplate, imaged for isotropic strain ($\varepsilon_{I,P}$), cooled to 20°C, and imaged for LC strain ($\varepsilon_{LC,P}$). Each data point was performed in triplicate, and SE was reported. All strains were reported relative to the initial "as-polymerized" shape of the LCE (ε_0).

Programming with gradient light (bending and folding)

Samples were made using a similar approach described above with the addition of Tinuvin 328 ultraviolet (UV) absorber in 0.5 wt % in the same manner as the photoinitiators. Bending was achieved by irradiating one face of a 250-μm-thick strip of LCE strained approximately 20% through a photomask (1-mm-thick line). The opposite face was then flood-irradiated, and the sample was thermally cycled. Images of the final bent state were taken, and the bending angle was determined using ImageJ (NIH).

Nanoscale imprinting and characterization

To impose diffraction-grating patterns on the surface of LCEs, we used an NIL system (Eitre 3, Obducat) to press a sample into a silicon mold, using a pressure of 3 MPa, while exposing them to UV light (300 to 400 nm, 20 mW/cm^2) for 1 min. The imprinting process extruded the LCE sample into the mold cavities while simultaneously using UV light to activate bond exchange; the process did not alter the material chemistry. To fix patterns in the LC phase, imprinting was done at 55°C, while a temperature of 99°C was used to program patterns in the isotropic state. To characterize the evolution of patterns during heating and cooling, a custom hot stage was placed into an AFM (Cypher S, Asylum Research) and imaged using the fast force-mapping technique (Nanosensors probe, PPP-SEIH-20). Three-minute equilibration time was allotted before scanning. No evidence of contamination or metal traces from the imprinting process was observed.

Diffraction measurements were taken by mounting the 25-μm-thick programmed sample onto a heating stage (Instec TS102). A HeNe laser (633 nm) was passed through the sample with the diffraction grating facing away from the laser resulting in three visible spots, two diffraction orders at approximately 50° angles, and transmission spot straight on. Two photodiodes (Newport visible sensors with silicon detectors) were placed in front of the transmission and one diffracted spot, and the corresponding intensities were recorded at various temperatures ranging from 30° to 99°C (±1°C). The diffraction efficiency is defined as the ratio of the intensity of the diffracted beam $I_{\text{diffracted}}$ to the intensity of the transmission beam $I_{\text{transmission}}$. Thus, diffraction efficiency here is defined as

$$\text{DE} = I_{\text{diffracted}}/I_{\text{transmission}} \times 100\%$$

Photopatterned alignment

Buckled features were developed by flood programming a strip of AFT-capable LCE into a monodomain, as described in the manuscript. A second erasing step was performed at 100°C with a photomask (250-μm–spaced 50-μm lines perpendicular to programmed alignment). The resulting polymer was analyzed with microscopy (Nikon Eclipse Ci) and profilometry (Dektak 6M).

Thermomechanical analysis and stress relaxation

Thermal cycling was performed by programming a 6 mm × 6 mm × 0.5 mm sample in the clamps of a TA RSA-G2 held at 80% strain and irradiated with 365 nm (30 mW/cm^2) for 180 s. The strain was removed, and the sample was then heated at 3°C/min to 100°C, then cooled to 28°C, and heated at 3°C/min to 100°C while maintaining 1 kPa of stress and monitoring the strain. Temperature-dependent mechanical properties of polydomain LCEs were measured on a TA RSA-G2 with 0.1 to 1% strain amplitude at 1 Hz and a heating rate of 3°C/min. A heating rate of 3°C/min was chosen to ensure uniform heating in reasonably timed experiments.

Stress relaxation experiments were performed in tension on the TA RSA-G2 with 10% strain for 10 min. Light (30 mW/cm^2 of 320 to 500 nm) was turned on after 5 min and remained on for the duration of the experiment.

SUPPLEMENTARY MATERIALS

Supplementary material for this article is available at http://advances.sciencemag.org/cgi/content/full/4/8/eaat4634/DC1

Fig. S1. Mechanism of allyl sulfide exchange.
Fig. S2. Thermomechanical analysis of LCEs.
Fig. S3. Reprogramming of the LC shape.
Fig. S4. A square peg morphs into a round peg when heated into the isotropic phase.
Fig. S5. Strain to break experiments for 1:0.5:1.35 RM82/NPGDA/allyl dithiol.
Fig. S6. Polarized optical microscopy of unprogrammed and programmed LCEs.
Fig. S7. Stress relaxation behavior of LCE at 120°C (gray), 67°C (blue), and 25°C (red).
Fig. S8. Heat coupled with light-erased programmed LC strain.
Fig. S9. Stress relaxation in the isotropic shape with and without load.

Fig. S10. Folded structure developed by programming each face separately.
Fig. S11. Patterned alignment results in surface topography.
Movie S1. A programmed LCE folds and unfolds during thermal cycling.
Movie S2. A square peg falling through a circular hole.

REFERENCES AND NOTES

1. C. A. Tippets, Q. Li, Y. Fu, E. U. Donev, J. Zhou, S. A. Turner, A.-M. S. Jackson, V. Sheares Ashby, S. S. Sheiko, R. Lopez, Dynamic optical gratings accessed by reversible shape memory. *ACS Appl. Mater. Interfaces* **7**, 14288–14293 (2015).
2. J. Kumar, L. Li, X. L. Jiang, D.-Y. Kim, T. S. Lee, S. Tripathy, Gradient force: The mechanism for surface relief grating formation in azobenzene functionalized polymers. *Appl. Phys. Lett.* **72**, 2096–2098 (1998).
3. C. J. Barrett, A. L. Natansohn, P. L. Rochon, Mechanism of optically inscribed high-efficiency diffraction gratings in azo polymer films. *J. Phys. Chem.* **100**, 8836–8842 (1996).
4. Y. H. Jiang, Q. M. Wang, Highly-stretchable 3D-architected mechanical metamaterials. *Sci. Rep.* **6**, 34147 (2016).
5. D. Liu, D. J. Broer, Light controlled friction at a liquid crystal polymer coating with switchable patterning. *Soft Matter* **10**, 7952–7958 (2014).
6. J. L. Silverberg, A. A. Evans, L. McLeod, R. C. Hayward, T. Hull, C. D. Santangelo, I. Cohen, Using origami design principles to fold reprogrammable mechanical metamaterials. *Science* **345**, 647–650 (2014).
7. C. M. Yakacki, M. Saed, D. P. Nair, T. Gong, S. M. Reed, C. N. Bowman, Tailorable and programmable liquid-crystalline elastomers using a two-stage thiol-acrylate reaction. *RSC Adv.* **5**, 18997–19001 (2015).
8. P. T. Mather, X. Luo, I. A. Rousseau, Shape memory polymer research. *Annu. Rev. Mater. Res.* **39**, 445–471 (2009).
9. A. Lendlein, H. Jiang, O. Jünger, R. Langer, Light-induced shape-memory polymers. *Nature* **434**, 879–882 (2005).
10. H. Finkelmann, E. Nishikawa, G. G. Pereira, M. Warner, A new opto-mechanical effect in solids. *Phys. Rev. Lett.* **87**, 015501 (2001).
11. T. F. Scott, R. B. Draughon, C. N. Bowman, Actuation in crosslinked polymers via photoinduced stress relaxation. *Adv. Mater.* **18**, 2128–2132 (2006).
12. T. J. White, N. V. Tabiryan, S. V. Serak, U. A. Hrozhyk, V. P. Tondiglia, H. Koerner, R. A. Vaia, T. J. Bunning, A high frequency photodriven polymer oscillator. *Soft Matter* **4**, 1796–1798 (2008).
13. A. H. Gelebart, G. Vantomme, E. W. Meijer, D. J. Broer, Mastering the photothermal effect in liquid crystal networks: A general approach for self-sustained mechanical oscillators. *Adv. Mater.* **29**, 1606712 (2017).
14. J. M. Boothby, H. Kim, T. H. Ware, Shape changes in chemoresponsive liquid crystal elastomers. *Sens. Actuators B Chem.* **240**, 511–518 (2017).
15. J. R. Kumpfer, S. J. Rowan, Thermo-, photo-, and chemo-responsive shape-memory properties from photo-cross-linked metallo-supramolecular polymers. *J. Am. Chem. Soc.* **133**, 12866–12874 (2011).
16. R. M. Baker, J. H. Henderson, P. T. Mather, Shape memory poly(ε-caprolactone)-*co*-poly (ethylene glycol) foams with body temperature triggering and two-way actuation. *J. Mater. Chem. B* **1**, 4916–4920 (2013).
17. A. S. Gladman, E. A. Matsumoto, R. G. Nuzzo, L. Mahadevan, J. A. Lewis, Biomimetic 4D printing. *Nat. Mater.* **15**, 413–418 (2016).
18. Q. Ge, H. J. Qi, M. L. Dunn, Active materials by four-dimension printing. *Appl. Phys. Lett.* **103**, 131901 (2013).
19. J. Ryu, M. D'Amato, X. Cui, K. N. Long, H. Jerry Qi, M. L. Dunn, Photo-origami—Bending and folding polymers with light. *Appl. Phys. Lett.* **100**, 161908 (2012).
20. H. Zeng, O. M. Wani, P. Wasylczyk, R. Kaczmarek, A. Priimagi, Self-regulating iris based on light-actuated liquid crystal elastomer. *Adv. Mater.* **29**, 1701814 (2017).
21. R. H. Baughman, Playing nature's game with artificial muscles. *Science* **308**, 63–65 (2005).
22. G. V. Stoychev, L. Ionov, Actuating fibers: Design and applications. *ACS Appl. Mater. Interfaces* **8**, 24281–24294 (2016).
23. Y. Zhang, F. Zhang, Z. Yan, Q. Ma, X. Li, Y. Huang, J. A. Rogers, Printing, folding and assembly methods for forming 3D mesostructures in advanced materials. *Nat. Rev. Mater.* **2**, 17019 (2017).
24. J. Küpfer, H. Finkelmann, Nematic liquid single crystal elastomers. *Meakromol. Chem. Rapid Commun.* **12**, 717–726 (1991).
25. D. J. Broer, H. Finkelmann, K. Kondo, In-situ photopolymerization of an oriented liquid-crystalline acrylate. *Makromol. Chem.* **189**, 185–194 (1988).
26. T. H. Ware, M. E. McConney, J. J. Wie, V. P. Tondiglia, T. J. White, Voxelated liquid crystal elastomers. *Science* **347**, 982–984 (2015).
27. T. J. White, D. J. Broer, Programmable and adaptive mechanics with liquid crystal polymer networks and elastomers. *Nat. Mater.* **14**, 1087–1098 (2015).
28. C. J. Kloxin, C. N. Bowman, Covalent adaptable networks: Smart, reconfigurable and responsive network systems. *Chem. Soc. Rev.* **42**, 7161–7173 (2013).
29. Y. Yang, Z. Pei, Z. Li, Y. Wei, Y. Ji, Making and remaking dynamic 3D structures by shining light on flat liquid crystalline vitrimer films without a mold. *J. Am. Chem. Soc.* **138**, 2118–2121 (2016).
30. Z. Pei, Y. Yang, Q. Chen, Y. Wei, Y. Ji, Regional shape control of strategically assembled multishape memory vitrimers. *Adv. Mater.* **28**, 156–160 (2016).
31. Z. Pei, Y. Yang, Q. Chen, E. M. Terentjev, Y. Wei, Y. Ji, Mouldable liquid-crystalline elastomer actuators with exchangeable covalent bonds. *Nat. Mater.* **13**, 36–41 (2014).
32. T. Ube, K. Kawasaki, T. Ikeda, Photomobile liquid-crystalline elastomers with rearrangeable networks. *Adv. Mater.* **28**, 8212–8217 (2016).
33. Y. Li, Y. Zhang, O. Rios, J. K. Keum, M. R. Kessler, Photo-responsive liquid crystalline epoxy networks with exchangeable disulfide bonds. *RSC Adv.* **7**, 37248–37254 (2017).
34. M. K. McBride, M. Hendrikx, D. Liu, B. T. Worrell, D. J. Broer, C. N. Bowman, Photoinduced plasticity in cross-linked liquid crystalline networks. *Adv. Mater.* **29**, 1606509 (2017).
35. D. W. Hanzon, N. A. Traugutt, M. K. McBride, C. N. Bowman, C. M. Yakacki, K. Yu, Adaptable liquid crystal elastomers with transesterification-based bond exchange reactions. *Soft Matter* **14**, 951–960 (2018).
36. M. O. Saed, R. H. Volpe, N. A. Traugutt, R. Visvanathan, N. A. Clark, C. M. Yakacki, High strain actuation liquid crystal elastomers via modulation of mesophase structure. *Soft Matter* **13**, 7537–7547 (2017).
37. S. V. Fridrikh, E. M. Terentjev, Polydomain-monodomain transition in nematic elastomers. *Phys. Rev. E* **60**, 1847–1857 (1999).
38. S. M. Clarke, A. R. Tajbakhsh, E. M. Terentjev, M. Warner, Anomalous viscoelastic response of nematic elastomers. *Phys. Rev. Lett.* **86**, 4044–4047 (2001).
39. Y. Meng, J.-C. Yang, C. L. Lewis, J. Jiang, M. Anthamatten, Photoinscription of chain anisotropy into polymer networks. *Macromolecules* **49**, 9100–9107 (2016).

Acknowledgments: We acknowledge C. Yakacki for the discussions. Certain commercial equipment, instruments, or materials are identified in this paper to specify the experimental procedure adequately. This identification does not imply recommendation or endorsement by National Institute of Standards and Technology, nor does it imply that the materials or equipment identified are necessarily the best available for the purpose. **Funding:** M.K.M. was funded by an NSF graduate fellowship (DGE 1144083), NSF CBET-1264298, NSF–Materials Research Science and Engineering Center DMR-1420736, NSF DMR-1310528, and NSF DMR-1809841. **Author contributions:** M.K.M. and C.N.B. developed the idea and devised experiments. M.K.M., A.M.M., M.P., and B.T.W. performed experiments. L.C. and J.K. performed and interpreted nanoimprinting and AFM. M.K.M., A.M.M., M.A., and K.C. performed and interpreted diffraction data. M.B. performed shape memory experiments. **Competing interests:** The authors declare that they have no competing interests. **Data and materials availability:** All data needed to evaluate the conclusions in the paper are present in the paper and/or the Supplementary Materials. Additional data related to this paper may be requested from the authors.

Submitted 1 March 2018
Accepted 17 July 2018
Published 24 August 2018
10.1126/sciadv.aat4634

Citation: M. K. McBride, A. M. Martinez, L. Cox, M. Alim, K. Childress, M. Beiswinger, M. Podgorski, B. T. Worrell, J. Killgore, C. N. Bowman, A readily programmable, fully reversible shape-switching material. *Sci. Adv.* **4**, eaat4634 (2018).

ScienceAdvances

A readily programmable, fully reversible shape-switching material

Matthew K. McBride, Alina M. Martinez, Lewis Cox, Marvin Alim, Kimberly Childress, Michael Beiswinger, Maciej Podgorski, Brady T. Worrell, Jason Killgore and Christopher N. Bowman

Sci Adv **4** (8), eaat4634.
DOI: 10.1126/sciadv.aat4634